

# Strain control of the Néel vector in Mn-based antiferromagnets

In Jun Park,<sup>1, a)</sup> Taehwan Lee,<sup>2</sup> Protik Das,<sup>1</sup> Bishwajit Debnath,<sup>1</sup> Greg P. Carman,<sup>3</sup> and Roger K. Lake<sup>1, b)</sup>

<sup>1)</sup>Department of Electrical and Computer Engineering, University of California, Riverside, CA 92521, USA

<sup>2)</sup>Department of Materials Science and Engineering, University of California, Los Angeles, CA 90095, USA

<sup>3)</sup>Department of Mechanical and Aerospace Engineering, University of California, Los Angeles, CA 90095, USA

(Dated: 26 November 2021)

Control of the Néel vector in antiferromagnetic materials is one of the challenges preventing their use as active device components. Several methods have been investigated such as exchange bias, electric current, and spin injection, but little is known about strain-mediated anisotropy. This study of the antiferromagnetic  $L1_0$ -type MnX alloys MnIr, MnRh, MnNi, MnPd, and MnPt shows that a small amount of strain effectively rotates the direction of the Néel vector by  $90^\circ$  for all of the materials. For MnIr, MnRh, MnNi, and MnPd, the Néel vector rotates within the basal plane. For MnPt, the Néel vector rotates from out-of-plane to in-plane under tensile strain. The effectiveness of strain control is quantified by a metric of efficiency and by direct calculation of the magnetostriction coefficients. The values of the magnetostriction coefficients are comparable with those from ferromagnetic materials. These results indicate that strain is a mechanism that can be exploited for control of the Néel vectors in this family of antiferromagnets.

There has been a rapidly increasing interest in the use of antiferromagnetic (AFM) materials for use as active device elements<sup>1–3</sup>. AFMs are insensitive to parasitic electromagnetic and magnetic interference. The dipolar coupling is minimal, since there is no net magnetic moment. Their lack of macroscopic magnetic fields allows AFM devices and interconnects to be highly scaled with reduced cross talk and insensitivity to geometrical anisotropy effects. AFM resonant frequencies and magnon velocities are several orders of magnitude higher than those in ferromagnetic materials, and these velocities correlate with similarly higher switching speeds<sup>3–5</sup>. AFM metals and insulators are plentiful, and many have Néel temperatures well above room temperature, a requirement for compatibility with on-chip temperatures in current Si integrated circuits.

The high Néel temperatures of the Mn-based equiatomic alloys such as MnIr, MnRh, MnNi, MnPd, and MnPt make them suitable candidates for on-chip applications<sup>1</sup>. Extensive research has been conducted on the electronic<sup>6–10</sup>, magnetic<sup>6,9–11</sup>, and elastic properties<sup>12,13</sup> of these materials. The spins on the Mn atoms are antiferromagnetically coupled with each other in the basal plane, and each plane is coupled ferromagnetically as shown in Fig. 1.

The positive attributes of speed, scaling, and robustness to stray fields are accompanied by the challenges of manipulating and detecting the antiferromagnetic states. There are several methods to control the magnetic properties of AFM materials such as with exchange bias<sup>1</sup>, the use of electric current<sup>14</sup>, and strain induced by a piezoelectric material<sup>15,16</sup>. The recent experimental demonstration of strain control of the Néel vector in MnPt<sup>16</sup>,

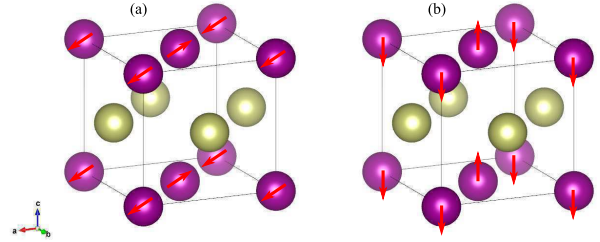


FIG. 1: Antiferromagnetic  $L1_0$ -type Mn alloy structures. Mn atoms are the purple spheres with the spin vectors, and the gold spheres indicate the Ir, Rh, Ni, Pd, or Pt atoms. (a) In-plane equilibrium spin texture of MnIr, MnRh, MnNi, and MnPd. (b) Out-of-plane equilibrium spin texture of MnPt.

provides timely motivation for a theoretical study of strain-mediated magnetic anisotropy in the MnX AFM materials. Density functional theory (DFT) is used to analyze the effect of strain on the magnetic anisotropy. The effectiveness of strain control is quantified by a metric of efficiency and by calculation of the magnetostriction coefficients.

First principles calculations are performed as implemented in the Vienna Ab initio Simulation Package (VASP)<sup>17</sup> to investigate the effect of strain on the magnetic anisotropy of  $L1_0$ -ordered bulk MnIr, MnRh, MnNi, MnPd, and MnPt. Projector augmented-wave (PAW) potentials<sup>18</sup> and the generalized gradient approximation (GGA) parameterized by Perdew-Burke-Ernzerhof (PBE) were employed<sup>19</sup>. Depending on the materials, different cut-off energies (typically ranging from 420 eV to 450 eV) and k-points grids were used in order to ensure the total energy converged within  $10^{-7}$  eV per unit cell. The initial equilibrium structure consists of a tetrag-

<sup>a)</sup>Electronic mail: ipark008@ucr.edu

<sup>b)</sup>Electronic mail: rlake@ece.ucr.edu

TABLE I: Calculated structure and local magnetic moment of the  $L1_0$ -type MnX alloys in the absence of strain.

	a (Å)	b (Å)	c (Å)	$\mu_{Mn}$ ( $\mu_B$ )
MnIr	3.84	3.84	3.64	2.8
MnRh	3.85	3.85	3.62	3.1
MnNi	3.62	3.62	3.58	3.2
MnPd	3.99	3.99	3.69	3.8
MnPt	3.98	3.98	3.71	3.7

onal unit cell where the fractional coordinates of Mn atoms are (0, 0, 0) and (0.5, 0.5, 0), and those of the X atoms are (0.5, 0, 0.5) and (0, 0.5, 0.5). Compressive or tensile stress along the  $a$  axis is applied to each structure, and the structure is fully relaxed along the  $b$  and  $c$  axes (biaxially) until all forces on each atom are less than  $10^{-4}$  eVÅ $^{-1}$ . The relaxed lattice constants for each applied strain are shown in supplementary Fig. S1. The strain is defined as, strain =  $(a - a_0)/a_0 \times 100\%$ , where  $a$  and  $a_0$  are the lattice constants with and without strain, respectively. With the relaxed structure, the spin-polarized self-consistent calculation is performed to obtain the charge density. Finally, the magnetic anisotropy energies are determined by calculating the total energies for different Néel vector directions including spin orbit coupling. Table I shows the lattice constants and the magnetic moments of the Mn site in MnX without strain. All of the values are very close to those from previous results<sup>12,13</sup>. The local magnetic moments of the X site are zero for all materials.

Figures 2–6 show the differences in the total energies as a function of the strain for MnIr, MnRh, MnNi, MnPd, and MnPt, respectively, where  $E_{abc}$  is the ground state energy with the Néel vector along the  $[abc]$  direction. The reference energy levels from each figure, which are indicated by the solid black lines, are  $E_{001}$  for MnPt and  $E_{110}$  for the other materials. The reference energies are the lowest energy state, which means MnIr, MnRh, MnNi, and MnPd have in-plane anisotropy and MnPt has out-of-plane anisotropy without strain. This is consistent with experimental results<sup>11</sup>. To show the energy differences more clearly as the strain changes, the reference level is taken at each value of the applied strain. At zero strain, there is no energy difference between  $E_{100}$  and  $E_{010}$  because of the symmetry of all of the materials.

Figures 2–5 show that sweeping the strain from negative (compressive) to positive (tensile) causes a 90° rotation of the Néel vector in the  $ab$ -plane for the four materials MnIr, MnRh, MnNi, and MnPd. However, the alignment of the Néel vector with compressive or tensile strain depends on the specific material. MnIr and MnRh behave like magnets with a positive magnetostriction coefficient, since tensile strain along  $[100]$  causes the Néel vector to align in the  $[100]$  direction. On the other hand, MnNi and MnPd behave like magnets with a negative magnetostriction coefficient, since tensile strain along  $[100]$  causes the Néel vector to align in the  $[010]$  direction<sup>20</sup>.

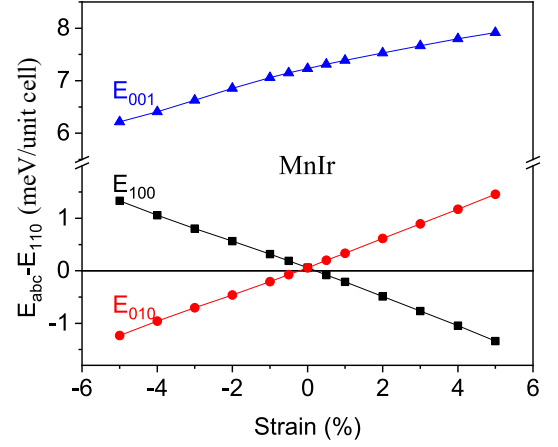


FIG. 2: MnIr energy differences  $E_{abc} - E_{110}$  for the 3 different orientations of the Néel vector as indicated by the labels.

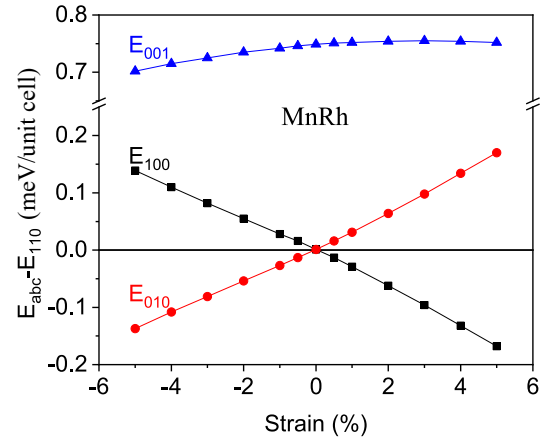


FIG. 3: MnRh energy differences  $E_{abc} - E_{110}$  for the 3 different orientations of the Néel vector as indicated by the labels.

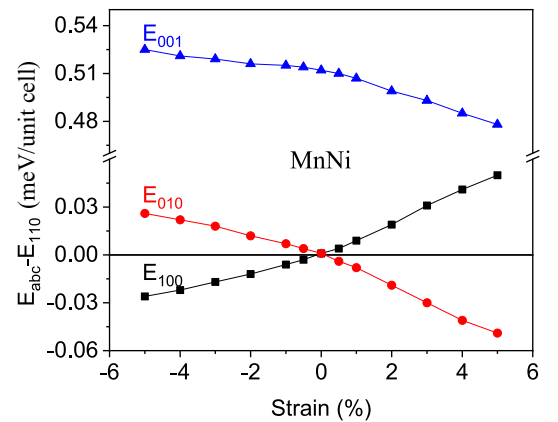


FIG. 4: MnNi energy differences  $E_{abc} - E_{110}$  for the 3 different orientations of the Néel vector as indicated by the labels.

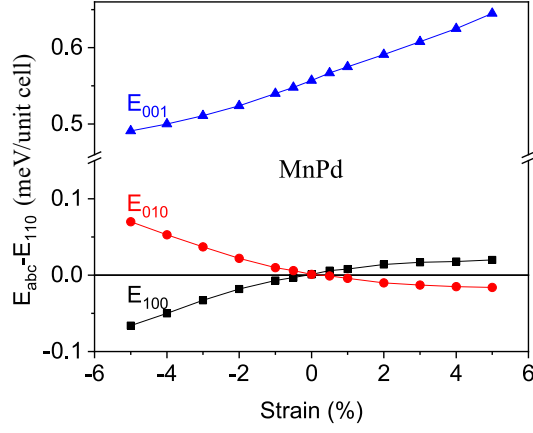


FIG. 5: MnPd energy differences  $E_{abc} - E_{110}$  for the 3 different orientations of the Néel vector as indicated by the labels.

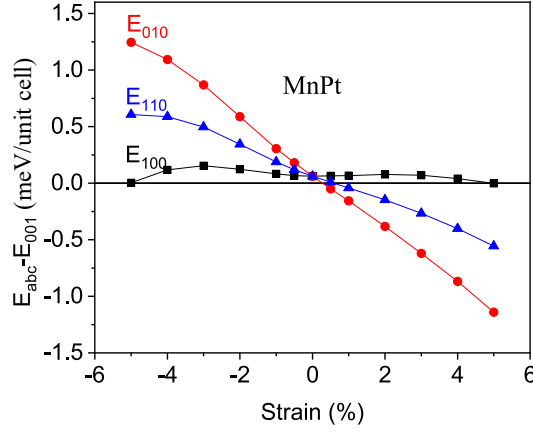


FIG. 6: MnPt energy differences  $E_{abc} - E_{110}$  for the 3 different orientations of the Néel vector as indicated by the labels.

MnPt is unique among the 5 materials. In equilibrium, in the absence of strain, the Néel vector has perpendicular anisotropy. Under compressive (negative) strain along the [100] axis, the Néel vector remains out-of-plane. Under tensile strain along [100], the Néel vector switches from out-of-plane [001] to in-plane aligning in the [010] direction.

For applications, it is useful to quantify the efficiency with which strain rotates the Néel vector and to determine the magnetostriction coefficient from the ab initio calculations. The internal efficiency is defined as

$$\text{Efficiency}(\%) = \left| \frac{E_{abc} - E_{a'b'c'}}{E_{\text{total}} - E_{\text{total}}(0)} \right| \times 100, \quad (1)$$

where the total energies  $E_{abc}$  and  $E_{a'b'c'}$  are defined in the same way as above, i.e. the total energies in the presence of strain with the Néel vector oriented along  $[abc]$  or  $[a'b'c']$ , respectively. The denominator in the Eq. (1) is the total energy change induced by the strain. For MnIr, MnRh, MnNi, and MnPd,  $E_{abc}$  and  $E_{a'b'c'}$  are

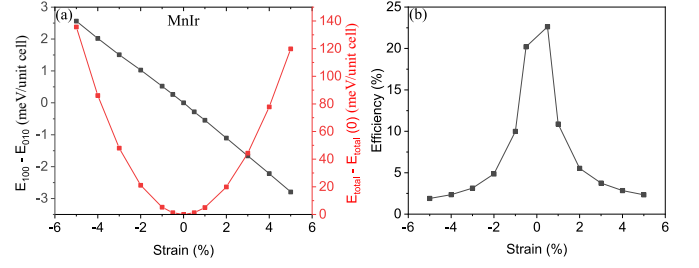


FIG. 7: MnIr strain energies and efficiency versus strain. (a) The energy difference between two different Néel vector orientations (black) as shown by the left axis, and the change in total energy (red) as shown by the right axis. (b) The efficiency as a function of the strain.

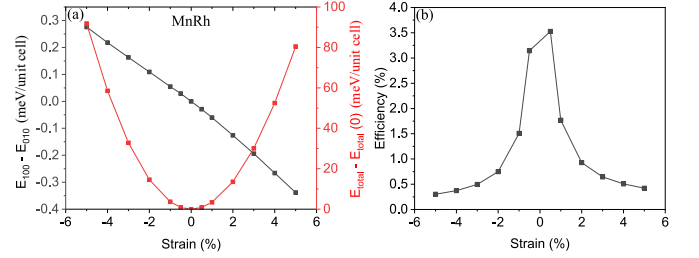


FIG. 8: MnRh strain energies and efficiency versus strain. (a) The energy difference between two different Néel vector orientations (black) as shown by the left axis, and the change in total energy (red) as shown by the right axis. (b) The efficiency as a function of the strain.

$E_{100}$  and  $E_{010}$ , respectively. For MnPt,  $E_{abc}$  and  $E_{a'b'c'}$  are  $E_{010}$  and  $E_{001}$ , respectively. The numerator and denominator of Eq. (1) are plotted as a function of strain in Figs. 7-11(a), and the resulting efficiencies are plotted as a function of strain in Figs. 7-11(b). The changes in the total energies, shown as red curves in Figs. 7-11(a), are parabolic so that they can be considered as the strain energy proportional to the square of the applied strain. On the other hand, the differences between two energies (the black curves in Figs. 7-11(a)) are approximately linear under small strain ( $< 1\%$ ). Therefore, the efficiency decreases sharply as the amount of strain

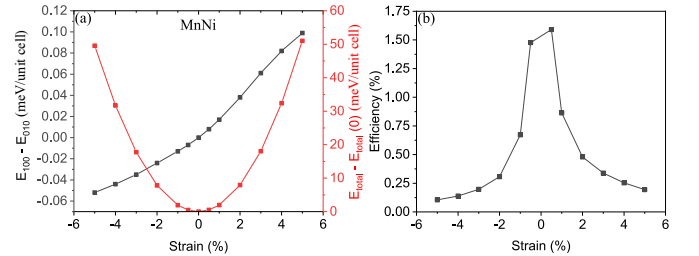


FIG. 9: MnNi strain energies and efficiency versus strain. (a) The energy difference between two different Néel vector orientations (black) as shown by the left axis, and the change in total energy (red) as shown by the right axis. (b) The efficiency as a function of the strain.

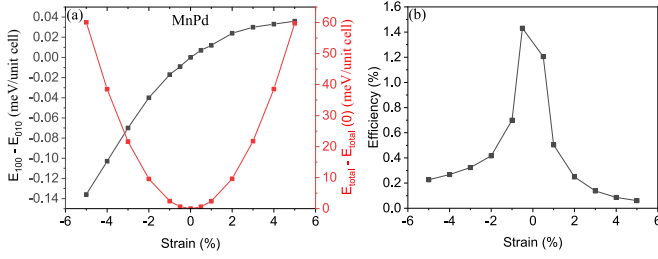


FIG. 10: MnPd strain energies and efficiency versus strain. (a) The energy difference between two different Néel vector orientations (black) as shown by the left axis, and the change in total energy (red) as shown by the right axis. (b) The efficiency as a function of the strain.

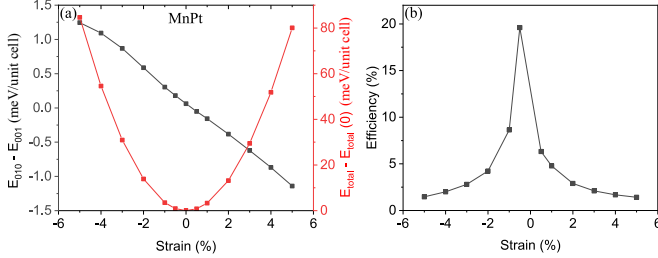


FIG. 11: MnPt strain energies and efficiency versus strain. (a) The energy difference between two different Néel vector orientations (black) as shown by the left axis, and the change in total energy (red) as shown by the right axis. (b) The efficiency as a function of the strain.

increases. At 0.5% strain, the highest efficiency for 90° in-plane rotation of the Néel vector is 20% for MnIr. For MnRh, MnNi, and MnPd, the efficiencies are smaller and equal to 3.5%, 1.5%, and 1.4%, respectively. To rotate the Néel vector from out-of-plane to in-plane in MnPt, a positive, tensile strain must be applied. The efficiency of this process at +0.5% strain is 6%.

Using the data above, the magnetostriction coefficients ( $\lambda_s$ ), which are widely used in ferromagnets, are calculated. The magnetostriction coefficient is defined as

$$\lambda_s(ppm) = \frac{2K_{me}}{3Y(\varepsilon_{bb} - \varepsilon_{aa})}, \quad (2)$$

where  $Y$  and  $(\varepsilon_{bb} - \varepsilon_{aa})$  are Young's modulus and strain, respectively<sup>21</sup>.  $K_{me}$  is the magnetoelastic anisotropy constant, which is defined as the difference of the magnetic anisotropy energies with and without strain, and the magnetic anisotropy energy is defined as  $E_{100} - E_{010}$ . Plots of  $E_{100} - E_{010}$  as a function of strain are shown in Supplementary Fig. S2. Young's moduli for all MnX alloys except MnIr were adopted from previous calculation results<sup>12,13</sup>, and the value for MnIr was determined as described in the Supplementary Information. For simplicity, we disregard  $\varepsilon_{bb}$  which represents a negligible change in the lattice constant along the  $b$ -axis caused by the applied strain along  $a$ . The results for  $\lambda_s$  are summarized in the Table II. As expected, MnIr and MnRh have posi-

tive values of  $\lambda_s$ , and MnNi, MnPd, and MnPt have negative values. Also, the magnitudes of the magnetostriction coefficients follow the magnitudes of the efficiencies. The magnetostriction coefficients of the MnX alloys are comparable with the ones from ferromagnets<sup>22–26</sup>, which suggests that strain can be used to control the magnetic anisotropy of these antiferromagnetic materials.

TABLE II: Calculated magnetostriction coefficients of the  $L1_0$ -type MnX alloys.

	MnIr	MnRh	MnNi	MnPd	MnPt
$\lambda_s$ (ppm)	241	43	-15	-17	-196

In summary, the Néel vectors of MnIr, MnRh, MnNi, and MnPd can be rotated 90° in the basal plane by applying in-plane strain. MnIr and MnRh behave like magnets with positive magnetostriction coefficients, since their Néel vectors align with tensile strain. MnNi and MnRh behave like magnets with negative magnetostriction coefficients, since their Néel vectors align with compressive strain. The internal efficiency of this process is highest for MnIr and it is equal to 20% at 0.5% strain. MnPt is unique among the 5 alloys in that its Néel vector aligns out-of-plane along the [001] axis in equilibrium. Applying a tensile strain along [100] rotates the Néel vector from out-of-plane [001] to in-plane [010]. The efficiency of this process at 0.5% tensile strain is 6%. Under compressive strain along [100], the Néel vector of MnPt remains out-of-plane [001]. The magnitudes of the calculated magnetostriction coefficients are comparable with those of ferromagnets, and they follow the same trends as the calculated efficiencies. For in-plane rotation of the Néel vector, MnIr has the highest magnetostriction coefficient of 241 ppm. The magnetostriction coefficient for out-of-plane rotation in MnPt is -196 ppm. These results suggest that strain can be an effective mechanism to control the Néel vectors in this family of antiferromagnets.

This work was supported as part of Spins and Heat in Nanoscale Electronic Systems (SHINES) an Energy Frontier Research Center funded by the U.S. Department of Energy, Office of Science, Basic Energy Sciences under Award #DE-SC0012670. This material is based upon work supported by or in part by the U.S. Army Research Laboratory and the U.S. Army Research Office under Grant No. W911NF-17-0364. This work used the Extreme Science and Engineering Discovery Environment (XSEDE)<sup>27</sup>, which is supported by National Science Foundation Grant No. ACI-1548562 and allocation ID TG-DMR130081.

<sup>1</sup>V. Baltz, A. Manchon, M. Tsoi, T. Moriyama, T. Ono, and Y. Tserkovnyak, Rev. Mod. Phys. **90**, 015005 (2018).

<sup>2</sup>O. Gomonay, T. Jungwirth, and J. Sinova, Physica Status Solidi (RRL) Rapid Research Letters **11**, 1700022 (2017).

<sup>3</sup>T. Jungwirth, X. Marti, P. Wadley, and J. Wunderlich, Nature Nanotechnology **11**, 231 (2016).

<sup>4</sup>E. V. Gomonay and V. M. Loktev, Low Temperature Physics **40**, 17 (2014).

- <sup>5</sup>C. Grezes, F. Ebrahimi, J. G. Alzate, X. Cai, J. A. Katine, J. Langer, B. Ocker, P. K. Amiri, and K. L. Wang, *Appl. Phys. Lett.* **108**, 012403 (2016).
- <sup>6</sup>A. Sakuma, *Journal of Magnetism and Magnetic Materials* **187**, 105 (1998).
- <sup>7</sup>R. Y. Umetsu, K. Fukamichi, and A. Sakuma, *Journal of magnetism and magnetic materials* **239**, 530 (2002).
- <sup>8</sup>R. Y. Umetsu, M. Miyakawa, K. Fukamichi, and A. Sakuma, *Physical Review B* **69**, 104411 (2004).
- <sup>9</sup>R. Y. Umetsu, K. Fukamichi, and A. Sakuma, *Materials transactions* **47**, 2 (2006).
- <sup>10</sup>R. Y. Umetsu, K. Fukamichi, and A. Sakuma, *Journal of the Physical Society of Japan* **76**, 104712 (2007).
- <sup>11</sup>L. Pál, E. Krén, G. Kádár, P. Szabó, and T. Tarnóczy, *Journal of Applied Physics* **39**, 538 (1968).
- <sup>12</sup>J. Wang, Z. Jiang, W. Chen, X. Zhang, and B. Zhou, *Intermetallics* **34**, 83 (2013).
- <sup>13</sup>J. Wang, A. Gao, W. Chen, X. D. Zhang, B. Zhou, and Z. Jiang, *Journal of Magnetism and Magnetic Materials* **333**, 93 (2013).
- <sup>14</sup>P. Wadley, B. Howells, J. Železný, C. Andrews, V. Hills, R. P. Campion, V. Novák, K. Olejník, F. Maccherozzi, S. S. Dhesi, *et al.*, *Science* **351**, 587 (2016).
- <sup>15</sup>A. Barra, J. Domann, K. W. Kim, and G. Carman, *Physical Review Applied* **9**, 034017 (2018).
- <sup>16</sup>H. Yan, Z. Feng, S. Shang, X. Wang, Z. Hu, J. Wang, Z. Zhu, H. Wang, Z. Chen, H. Hua, *et al.*, *Nature Nanotechnology* **14**, 131 (2019).
- <sup>17</sup>G. Kresse and J. Hafner, *Physical Review B* **47**, 558 (1993).
- <sup>18</sup>P. E. Blöchl, *Physical Review B* **50**, 17953 (1994).
- <sup>19</sup>J. P. Perdew, K. Burke, and M. Ernzerhof, *Physical Review Letters* **77**, 3865 (1996).
- <sup>20</sup>A. K. Biswas, S. Bandyopadhyay, and J. Atulasimha, *Applied Physics Letters* **104**, 232403 (2014).
- <sup>21</sup>A. Bur, T. Wu, J. Hockel, C. J. Hsu, H. K. D. Kim, T. K. Chung, K. Wong, K. L. Wang, and G. P. Carman, *Journal of Applied Physics* **109**, 123903 (2011).
- <sup>22</sup>A. E. Clark, J. B. Restorff, M. Wun-Fogle, T. A. Lograsso, and D. L. Schlager, *IEEE Transactions on Magnetics* **36**, 3238 (2000).
- <sup>23</sup>M. K. Panduranga, T. Lee, A. Chavez, S. V. Prikhodko, and G. P. Carman, *AIP Advances* **8**, 056404 (2018).
- <sup>24</sup>R. C. Hall, *Journal of Applied Physics* **30**, 816 (1959).
- <sup>25</sup>J. Huang, C. Prados, J. E. Evetts, and A. Hernando, *Physical Review B* **51**, 297 (1995).
- <sup>26</sup>D. Fritsch and C. Ederer, *Physical Review B* **86**, 014406 (2012).
- <sup>27</sup>J. Towns, T. Cockerill, M. Dahan, I. Foster, K. Gaither, A. Grimshaw, V. Hazlewood, S. Lathrop, D. Lifka, G. D. Peterson, *et al.*, *Computing in Science & Engineering* **16**, 62 (2014).

# Strain control of the Néel vector in Mn-based antiferromagnets: Supplementary Information

In Jun Park\*

*Department of Electrical and Computer Engineering,  
University of California, Riverside, CA 92521, USA*

Taehwan Lee

*Department of Materials Science and Engineering,  
University of California, Los Angeles, CA 90095, USA*

Protik Das and Bishwajit Debnath

*Department of Electrical and Computer Engineering,  
University of California, Riverside, CA 92521, USA*

Greg P. Carman

*Department of Mechanical and Aerospace Engineering,  
University of California, Los Angeles, CA 90095, USA*

Roger K. Lake<sup>†</sup>

*Department of Electrical and Computer Engineering,  
University of California, Riverside, CA 92521, USA*

(Dated: November 26, 2021)

Figure S1 shows the change in the lattice constants in MnX alloys as a function of applied strain along the  $a$  axis. The  $a$  lattice parameter is linearly increased and the  $b$  and  $c$  lattice constants are relaxed. In figure S2, we show the calculated values of  $K_{me}$  evaluated at all values of strain and make a linear fit to extract the slope, which is used as the term  $\frac{K_{me}}{\varepsilon_{bb}-\varepsilon_{aa}}$  in the Eq. (2) in the main text. As mentioned in the main paper, the Young's moduli were taken from previous results.<sup>1,2</sup> However, we were unable to find any values for the Young's modulus of MnIr. To calculate the magnetostriction coefficient for MnIr, we adopted the bulk modulus from Materials Project<sup>3</sup> and used the relation  $Y(GPa) = 3K(1-2\nu)$  where  $Y$ ,  $K$ , and  $\nu$  are the Young's modulus, bulk modulus, and Poisson's ratio, respectively.

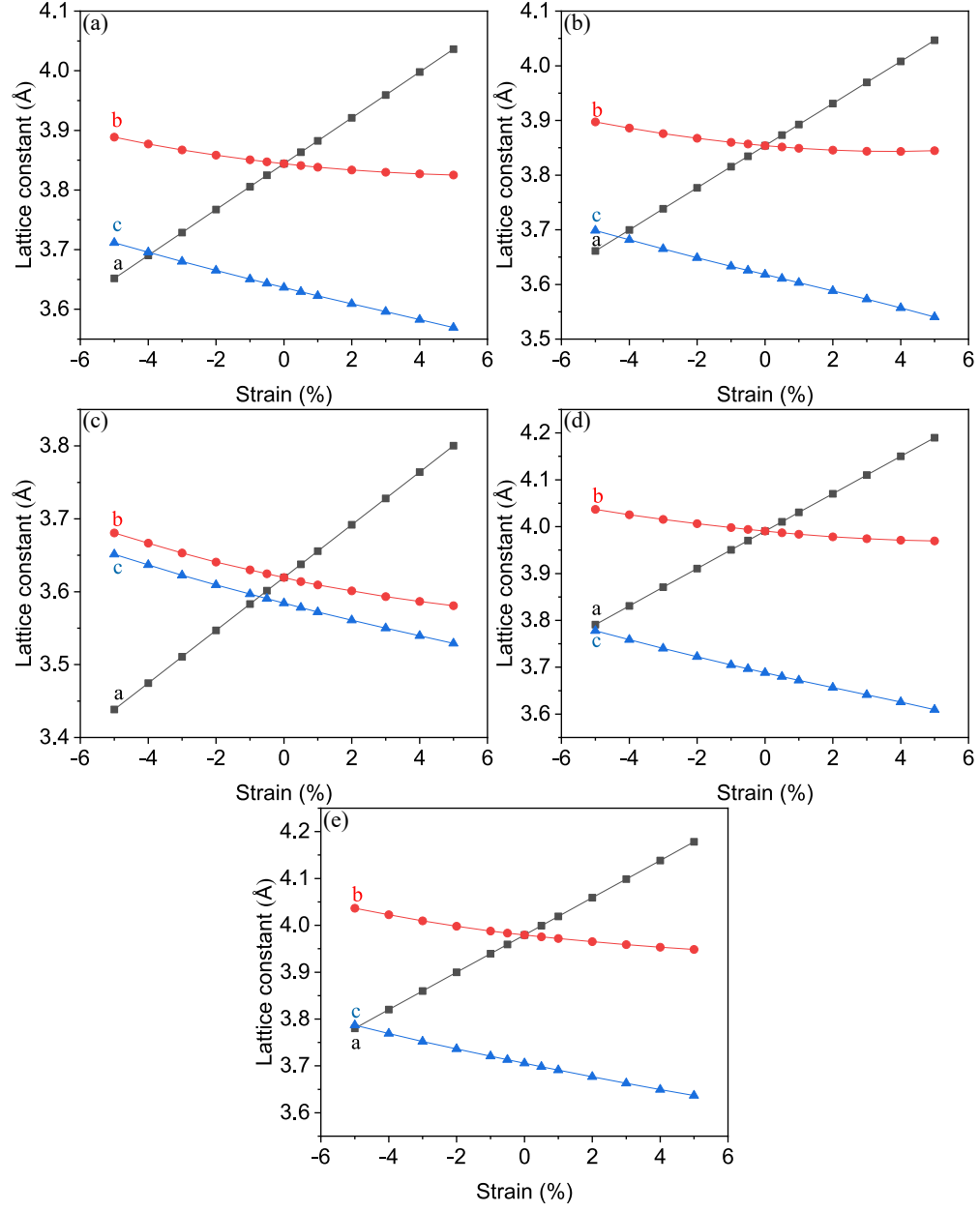


FIG. S1: The lattice constants versus applied strain in (a) MnIr, (b) MnRh, (c) MnNi, (d) MnPd, and (e) MnPt.



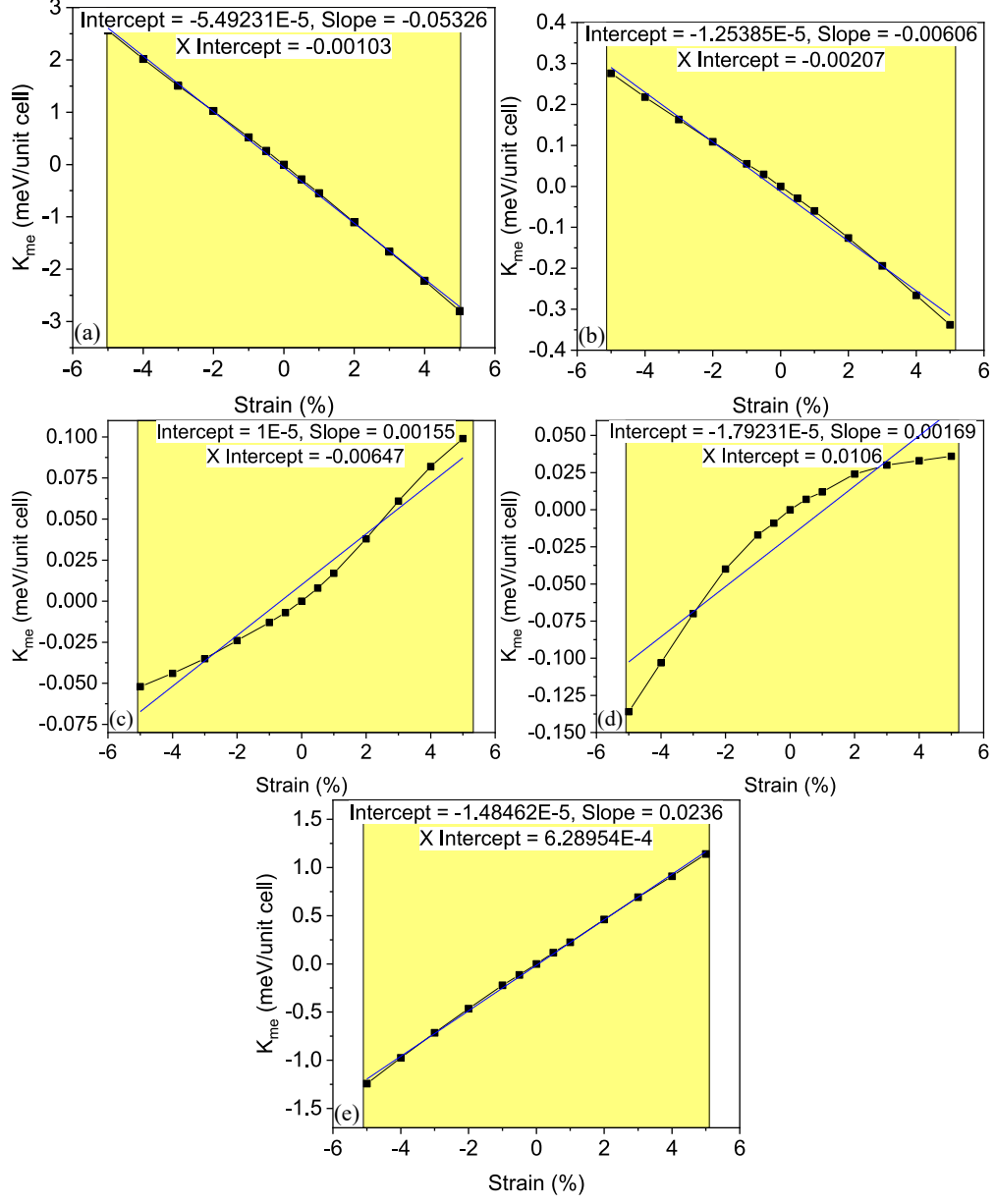


FIG. S2: The magnetoelastic anisotropy constants versus applied strain in (a) MnIr, (b) MnRh, (c) MnNi, (d) MnPd, and (e) MnPt.

---

\* ipark008@ucr.edu

† rlake@ece.ucr.edu

- <sup>1</sup> J. Wang, Z. Jiang, W. Chen, X. Zhang, and B. Zhou, “The first-principles study of martensitic transformations in MnMe (Me= Rh, Pd) alloys at low temperatures,” *Intermetallics* **34**, 83–88 (2013).
- <sup>2</sup> J. Wang, A. Gao, W. Chen, X. D. Zhang, B. Zhou, and Z. Jiang, “The structural, elastic, phonon, thermal and electronic properties of MnX (X= Ni, Pd and Pt) alloys: First-principles calculations,” *Journal of Magnetism and Magnetic Materials* **333**, 93–99 (2013).
- <sup>3</sup> “Materials Project,” <https://materialsproject.org/materials/mp-1670/>, accessed: 2019-02-13.